NASA TECHNICAL MEMORANDUM

NASA TM-73748

NASA TM-73748

MEASUREMENT OF FAR FIELD COMBUSTION NOISE FROM A TURBOFAN ENGINE USING COHERENCE FUNCTIONS

by A. M. Karchmer, M. Reshotko, and F. J. Montegani
Lewis Research Center
Cleveland, Ohio 44135

TECHNICAL PAPER to be presented at the
Fourth Aeroacoustics Conference
sponsored by the American Institute of Aeronautics and Astronautics
Atlanta, Georgia, October 3-5, 1977

MEASUREMENT OF FAR FIELD COMBUSTION NOISE FROM A TURBOFAN ENGINE USING COHERENCE FUNCTIONS

by A. M. Karchmer, M. Reshotko, and F. J. Montegani

National Aeronautics and Space Administration
Lewis Research Center
Cleveland, Ohio 44135

ABSTRACT

Coherence measurements between fluctuating pressure in the combustor of a YF-102 turbofan engine and far-field acoustic pressure were made. The results indicated that a coherent relationship between the combustor pressure and far-field existed only at frequencies below 250 Hz, with the peak occurring near 125 Hz. The coherence functions and the far-field spectra were used to compute the combustor-associated far-field noise in terms of spectra, directivity, and acoustic power, over a range of engine operating conditions. The acoustic results so measured were compared with results obtained by conventional methods, as well as with various semiempirical predictions schemes. Examination of the directivity patterns indicated a peak in the combustion noise near 120° (relative to the inlet axis).

E-9320

INTRODUCTION

Most attempts to date to measure the combustion noise contribution from operating turbofan engines have been restricted to acoustic measurements made entirely outside the engine (refs. 1 and 2, for example). The usual procedure is to make a series of far-field acoustic measurements at progressively lower engine power settings. The data are then

STAR Category 71
AIAA Paper No. 77-1277

examined for behavior not characteristic of jet mixing noise (e.g., sound power not proportional to jet velocity to the eighth power, improper Strouhal scaling of spectra, etc.). The observed differences are then attributed to "internal" or core noise sources. A similar approach, in combination with internal measurements, was reported by two of the present authors in reference 3 (for the same engine to be reported on in this paper). This technique, however, is unable to qualitatively distinguish one internal noise source from another.

Alternatively, internal pressure and external acoustic measurements can be used in conjunction with cross-correlation techniques. This can provide useful diagnostic source information (refs. 4 and 5). The time domain information by itself, though, is insufficient to quantify the source contribution to the acoustic far-field. In reference 6 the results of a series of diagnostic measurements conducted on an AVCO-Lycoming YF-102 turbofan engine were reported. There, the phase and amplitude relations between internal pressures and between internal and far-field acoustic pressures were examined by Fourier-transforming the corresponding cross-correlation functions. The results indicated that the combustor could be identified as a source region for far-field sound. Additionally, the measured coherence functions between combustor pressure and far-field acoustic pressure indicated that the combustor-associated far-field noise was limited to frequencies below 250 Hz, with a peak occurring near 125 Hz. In this paper, the quantitative contribution of the combustor to overall engine noise in terms of sound pressure level spectra, directivity, and acoustic power will be reported.

ENGINE, INSTRUMENTATION, DATA PROCESSING

Engine and Test Site

The test program was conducted on an AVCO-Lycoming YF-102 turbofan engine which has a bypass ratio of 6 and a rated thrust of 33 kN. This engine has a 1 m diameter fan and a core consisting of 7 axial com-

pressor stages, 1 centrifugal compressor stage, a reverse-flow annular combustor, and a four-stage turbine. The exit diameter of the core nozzle was 42 cm and the engine was operated with a bellmouth inlet. A cutaway illustration of the engine is shown in figure 1.

All tests were conducted at an outdoor acoustic test site with a hard surface ground plane. The engine was suspended from the test stand with its centerline 2.9 m above the ground plane (fig. 2). The far-field microphone array consisted of sixteen 1.27 cm diameter condenser microphones placed on a 30.5 m radius arc centered approximately 1.2 m upstream of the primary nozzle exit plane. The microphones were spaced 10^{o} apart from 10^{o} to 160^{o}, measured from engine inlet axis. All microphones were mounted at ground level to minimize problems associated with ground reflections, and were fitted with windscreens.

Test Conditions

Simultaneous internal (i.e., core) fluctuating pressure and far-field acoustic measurements were made at eight different fan speeds at approximately equal intervals between 30 and 95 percent of maximum speed (7600 rpm). The corresponding range of combustor temperatures and core jet exhaust velocities were from 810 K, 98 m/sec to 1375 K, 314 m/sec.

Internal Probes

The dynamic pressure measurements within the engine core were made simultaneously with the far-field acoustic pressure measurements and at seven different locations as shown in figure 3. Their number and locations were: two just downstream of the compressor exit about 2 cm apart; one at the combustor inlet; two within the annular combustor itself, both at the same axial location but separated 90^{o} circumferentially; and two within the core nozzle, one just downstream of the turbine at the nozzle entrance and one close to the nozzle exit plane.

This paper, however, will report the results obtained from the coherence measurements between just the in-line combustor probe and the far-field microphones. Spectral data from the other internal probes, as well as additional far-field data may be found in reference 3.

The transducers used for the internal pressure measurements were conventional 0.635 cm condenser microphones with pressure response cartridges. To avoid direct exposure of the microphones to the severe environment within the core, they were mounted outside the engine and the fluctuating static pressure in the engine core was communicated to the transducers by means of a "semi-infinite" acoustic waveguide.

A drawing of a typical probe is shown in figure 4. The microphone was flush mounted in the acoustic waveguide through a supporting block and housed in a pressure chamber. Attached to the block were a 0.635 cm diameter sensing tube on one end and a coil of tubing of the same diameter, 30 m long, on the other. The sensing tube of each probe was flush mounted as a static pressure tap at each of the various measuring locations within the engine core. A regulated nitrogen purge flow was maintained in the sensing line to protect the microphone from hot core gases. Static pressure was balanced across the microphone by means of a small vent hole connecting the pressure chamber and sensing line. Ambient temperature calibration tests of these probes indicated a flat frequency response within ±2 dB and a phase response of $\pm 5^{o}$ up to 1500 Hz. Additional details on these probes and their installation are also contained in reference 3.

Data Acquisition and Processing

The signals from the internal probes and far-field microphones were FM-recorded on magnetic tape in 2-minute record lengths for later processing. The internal probes and far-field microphones were calibrated with a pistonphone prior to and at the end of each day's running.

The results given in this paper were obtained by off-line processing of the taped data on a two-channel fast Fourier transform digital signal processor with built-in a-d converters and 120 dB/octave anti-aliasing

filters. The processor was capable of direct computation of up to 4096 ensemble averages of a 1024 point forward or inverse Fourier transform to yield either time-domain (correlation) or frequency domain (amplitude and phase spectra, transfer function, and coherence) information. No corrections were applied to the results obtained to account for atmospheric attenuation. However, at the low frequencies involved (generally less than about 250 Hz) such corrections would be negligible. Additionally, corrections to standard day conditions were not made. The computed combustor coherence spectra (and resulting directivity) were not corrected to free-field conditions and, as such, are "as measured." Finally, the combustor coherence spectral levels were normalized on a spectral density basis and their amplitudes are in terms of dB/Hz.

RESULTS

Coherence Functions

The tool to be used here in quantifying the combustor contribution is the ordinary coherence function. Basically, this function is a normalized cross-spectrum and is defined for random functions as:

$$\gamma^2_{xy}(\omega) = \frac{|G_{xy}(j\omega)|^2}{G_{xx}(\omega)G_{yy}(\omega)} \qquad (j = \sqrt{-1})$$

where $\omega = 2\pi f$

f = frequency

Here, $\gamma^2_{xy}(\omega)$ is the ordinary coherence function between two signals, say x and y. $|G_{xy}(j\omega)|^2$ is the square of the ensemble averaged value of the cross-spectrum between x and y; and $G_{xx}(\omega)$ and $G_{yy}(\omega)$ are the averaged values of the autospectra of x and y, respectively.

The coherence function is essentially the frequency domain analog of the cross-correlation function with high (low) coherence at a particular frequency indicating high (low) correlation at that frequency. Under the

appropriate circumstances the numerical value of the coherence may be interpreted as a measure of the fractional portion of the output of a system which is contributed by a particular input, at a particular frequency. The assumptions involved in such an interpretation, as well as the implications in the present context will be discussed in a later section of this paper.

The measured coherence function between the fluctuating combustor pressure and the 120^{o} far-field acoustic pressure is shown in figure 5. These data are for an engine operating condition of 43 percent of maximum speed. It can be clearly seen that there is no (linear) relationship between the fluctuating combustor pressure and the far-field acoustic pressure at frequencies beyond about 250 Hz. The frequency of peak coherence occurs near 125 Hz.

Figure 5 is presented for an analysis range from 0 to 1 kHz to graphically illustrate the lack of coherence between combustor pressure and far-field acoustic pressure beyond about 250 Hz. This qualitative result was found to prevail at all microphone angles and all engine operating conditions. The remaining coherence functions to be shown, therefore, will be presented to 400 Hz only. This frequency was chosen to avoid a significant bias error in the numerical value of the coherence, which is due to the natural propagation delay time between the two signals. The nature of this bias error when analyzing at higher frequencies is discussed in the appendix.

The coherence functions between the combustor pressure and the 120^{o} far-field acoustic pressure are shown in figures 6(a) to (f), for six engine operating speeds of 30, 37, 43, 50, 60, and 75 percent, respectively. With only minor variations, and excluding an occasional isolated spike, the frequency of the coherence peak remains fixed near 100-125 Hz for each of the operating speeds up to 60 percent. Further, the value of the peak coherence decreases slowly from a maximum of about 0.62 at 30 percent speed to about 0.32 at 50 and 60 percent speed, and then virtually to zero at 75 percent speed. This slow decrease in coherence is due to the increasing contribution of the other engine noise sources in the far-field, especially the jet noise, as engine speed is increased.

This is in qualitative agreement with the results given in reference 3, where it is shown that for this engine the core noise (as opposed to just the combustion noise) is apparent in the far-field data up to about 60 percent of maximum speed after which the jet mixing noise begins to dominate.

As indicated, similar results were obtained at other angles. In figures 7(a) and (b), for example, are shown the measured coherence functions between combustor and far-field pressures at far-field angles of 60^{o} and 160^{o}, for an engine speed of 43 percent of maximum. The envelopes of these functions are qualitatively similar. However the coherence at the 60^{o} angle is seen to have several pronounced dips at frequencies of about 80, 120, 160, and 200 Hz. These dips occurred consistently at these frequencies at the forward arc angles near 60^{o} and resulted in an unusual directivity pattern for these frequencies, as will be shown.

Combustor Coherence Spectra and Directivity

Subject to certain assumptions, the numerical value of the ordinary coherence functions shown above can be interpreted as the fraction of the far-field acoustic signal contributed by the combustor. A frequency-by-frequency multiplication, therefore, of the appropriate coherence function and the corresponding far-field spectrum produces the spectral contribution of the combustor associated noise in the far-field, here called the combustor coherence spectrum.*

The far-field sound pressure level spectral densities at 60^{o}, 120^{o}, and 160^{o} are shown in figures 8(a), (b), and (c) (dashed curves), respectively, for an engine operating speed of 43 percent. The resulting combustor coherence spectra at these angles are shown by the solid curves on the same figure. These were obtained by multiplication of the far-

*In the literature dealing with random data analysis, this quantity is often referred to as the coherent output power. However, to avoid confusion with the physical quantity of acoustic power, to be shown in a later section, the result of this multiplication will be called the combustor coherence spectrum.

field spectra by the corresponding coherence functions shown in figures 7(a), 6(c), and 7(b), respectively.

The primary observation to be made is that, because the far-field acoustic spectra are relatively flat, the combustor coherence spectra peak approximately at the same frequency as the coherence functions themselves, around 125 Hz. Also, as first suggested from the coherence functions, the results indicate that there is virtually no combustor-associated far-field noise at frequencies beyond about 200-250 Hz. This is about two full octaves below the frequency range most often suggested by other investigators as being associated with combustion noise from more conventional turbofan engines; that is, peak frequencies nearer to 400 to 500 Hz.

The above procedure was repeated for each operating condition from 30 percent speed to 60 percent speed, and for each far-field angle from 40^{o} to 160^{o}. The overall sound pressure level (OASPL) at each angle and operating condition was then obtained by numercially integrating the combustor coherence spectra. A 20 Hz integrating increment was used. Three of the resulting directivity patterns are shown in figure 9, for operating speeds of 30, 43, and 60 percent. A modest increase in OASPL at each angle is observed with increasing engine speed. The radiation patterns, however, appear to remain constant as engine speed is increased, each showing a slight peak near 120^{o}. This is consistent with results found by other investigators (refs. 7, 8, 9, for example). Similar results were obtained for the intermediate engine speed settings of 37 and 50 percent.

Because the radiation patterns remain invariant with engine power setting, it is convenient to normalize them into a single directivity index curve. The result, arithmetically averaged over the five engine operating speeds between 30 and 60 percent is shown in figure 10 as the open symbols. For comparison, the directivity index obtained from the empirical prediction schemes of references 7, 8, and 9 are also shown. The present results are seen to be in remarkably close agreement with the empirical prediction of reference 7. The prediction procedure recommended in reference 8 appears to underpredict the directivity index

found here at forward and rearward angles near the axis. The procedure of reference 9 produces results which somewhat overpredict the directivity index at the rearward angles. However, in the range between about 60^{o} and 130^{o}, the results found here agree reasonably well with the directivities of all three prediction schemes.

In reference 3, it was shown that the far-field data at engine speeds below about 60 percent were due primarily to core noise sources. To the extent that core noise in general, and combustion noise in particular have the same radiation patterns, the radiation patterns obtained from the combustor coherence spectra should agree with the low frequency radiation patterns obtained by direct far-field measurement. This comparison is shown in figure 11. The directivity index shown for the far-field data was obtained by summing the 1/3-octave band far-field sound pressure levels in the bands at center frequencies from 50 to 200 Hz. The far-field result is for the single operating condition of 43 percent engine speed. The data are seen to compare extremely well through all angles at which coherence measurements are available. No coherence data was available at angles of 10^{o}, 20^{o}, and 30^{o} because of limitations in the number of available tape recording channels.

Although the OASPL directivities were found to agree reasonably well with those of most previous studies, the same was not true of the directivity patterns associated with certain frequencies. In figures 7(a) and 8(a), for example, pronounced dips in the measured coherence function and corresponding combustor coherence spectrum are clearly shown. However, for the most part these dips gradually disappeared at angles away from 60^{o}. This resulted in unusual directivity patterns for frequencies of 80, 120, 160, and 200 Hz as is shown in figure 12. Figure 12 contains the data for an operating speed of 43 percent. However similar results were found for these same frequencies at all speeds through 30 percent. These results imply the presence of a noise source at these frequencies which does not correlate with the combustor pressures, but which is highly directional. Such a directional pattern seems irreconcilable with the low frequencies associated with it. It may also, however, result from some unusual phasing relationship between direct

radiation and casing radiation, or between radiation from the nozzle and radiation from the bellmouth inlet. Precisely the same result was observed when the tests were rerun about 10 days later. The possibility, therefore, of an isolated anomalous test condition is remote.

Power Levels

Acoustic power spectra were also obtained by numerically integrating spacially the combustor coherence spectra. Three of these acoustic power spectra are shown in figure 13 for the engine operating speeds of 30, 43, and 60 percent. The acoustic power spectral shapes are seen to vary somewhat as operating speed increases, with the primary differences occurring at frequencies beyond the peak. There appears to be a trend towards a slightly increasing peak frequency with engine operating speed, but this may be an artifact of the relatively large bandwidth (20 Hz) chosen for the numerical integration.

The integrated overall sound power level (OAPWL) is shown for each spectrum in figure 13 (corrected for time delay bias, see appendix). Table I below presents a comparison of the present results with the acoustic power predicted by the schemes of references 7, 8, and 9. The data in the column labeled "Direct Far-Field Measurement" were obtained by summing the far-field 1/3-octave band power levels from 50 to 200 Hz. The coherence results are seen to agree reasonably well with the prediction of reference 8 but are considerably less than those of references 7 and 9, or the directly measured far-field results.

DISCUSSION OF RESULTS

The results shown above indicate that at all angles and operating conditions for this engine, there is no combustor associated far-field noise at frequencies above about 250 Hz. Further, the peak frequency of the combustor associated noise is near 125 Hz. This is approximately two full octaves below the frequency range most often suggested by other investigators as being associated with combustion noise from more con-

ventional turbofan engines; that is, peak frequencies near 400 to 500 Hz. In this section, the possible reasons for the decorrelation of pressures between combustor and far-field will be discussed.

In general, there are three possible situations that can exist that would result in the ordinary coherence function having a value less than unity (10).

(a) The output is due to inputs in addition to, or other than, the input being measured. That is, there is "noise" at the output.

(b) There is extraneous "noise" (i.e., contamination) at the input which does not correlate with the output.

(c) The system relating the "input" (in this case the combustor pressure) to the "output" (in this case the far-field acoustic pressure) is nonlinear.

Case (a) is considered first. In the present application there clearly are contributions to the output from inputs other than what is being measured. Specifically, these other inputs are the mixing noise from the core and fan jet exhausts, broadband turbine noise, scrubbing noise within the core and fan nozzles, and other core noise sources. These, of course, are precisely the noises from which we are trying to distinguish the combustion noise and so do not represent "noise" in the sense above.

Case (b) involves a more subtle point. In reference 11 the authors point out that the presence of nonpropagating hydrodynamic pressure fluctuations (i.e., pseudosound) within the combustor and detected by the internal pressure transducer would serve to reduce the pressure coherence between the combustor and acoustic far-field. The conclusion in reference 11 is that this reduced coherence is not necessarily indicative of a correspondingly reduced combustion noise contribution to the far-field. Based on this conclusion, therefore, it may be argued that this pseudosound "contamination" is responsible for the lack of any pressure coherence between combustor and far-field beyond 250 Hz.

It is the view of the present authors, however, that in a source region this distinction between acoustic pressures and nonacoustic pressures loses its meaning. In the present work the causal relationship

between the fluctuating pressure in the source region, whatever its nature, and the acoustic far-field is being investigated. As such, the entire pressure field in the combustor is of interest and not just those pressures which can be specifically identified as being locally acoustic in their character. The issue of nonpropagating fluctuating hydrodynamic pressure "contamination" in the combustor pressure measurement, therefore, is not meaningful in the present context.

The issue of nonlinearity, case (c), is more difficult to address. In all the results which have been presented, there has been an implicit assumption that the acoustic propagation mechanism between combustor and far-field is linear. It would appear likely that if nonlinearities exist they would be due to the high pressure levels which exist in the combustor. In reference 3 several combustor pressure spectra were shown for this engine. At 43 percent engine speed, the pressure level reported at 250 Hz was about 118 dB (re. 2×10^{-5} Pa) normalized to a one Hz bandwidth. It does not seem reasonable that this pressure level is sufficiently high to result in completely nonlinear propagation. Nevertheless, without a detailed knowledge of the propagation phenomena between combustor and far-field, the presence of nonlinear effects must be admitted as at least being possible.

There is, however, supporting evidence for the spectral results shown above. In reference 12 the authors report the results of a combustion noise investigation on a turboshaft auxiliary power unit, with the turbine removed. The results presented in reference 12, obtained from far-field acoustic measurements only, indicate a clear combustion noise peak at 125 Hz in the acoustic power level spectrum. Further, at 250 Hz, the power level is down approximately 10 dB (after adjusting the data in (12) to a constant bandwidth basis, as used here. In reference 12 the data are presented in full octave bands). This result is not inconsistent with the results shown above.

The final point to be addressed here is the question of whether or not the single point pressure measurement in the combustor is adequate to characterize the entire source region. That is, there may be several (or perhaps, many) independent source regions within the combustor,

each contributing to the far-field noise. If this were the case then the coherence function between a single the combustor pressure measurement and the far-field acoustic pressure would be reduced. (Note that this is really an extension of case (a) above.) Consequently, the combustor coherence spectrum would not include the contributions from the other combustor source regions and hence its amplitude would be underestimated. The previous result, for example, showed that the overall power levels computed via the coherence functions were about 5-8 dB less than those computed by integrating the low frequency far-field spectra.

It does not appear likely, however, that the existence of multiple independent source regions is responsible for all of this difference. For example, from figure 6(a), the peak coherence between combustor pressure and far-field acoustic pressure is seen to be about 0.62 at the peak frequency. After correcting this value to account for time delay bias (see appendix), a closer estimate of the value of the coherence at this frequency is about 0.72. So at the peak frequency, approximately 72 percent (i.e., within 1.5 dB) of the far-field signal can be accounted for by a single point pressure measurement in this combustor.

Operating on the notion that low frequency information tends to remain correlated over larger volumes than high frequency information, it is concluded that a single point combustor measurement that is very nearly adequate to characterize the source region at the peak frequency must also be valid at frequencies below the peak. Conversely, we would expect this conclusion to be less valid at frequencies beyond the peak. However, again citing the evidence of reference 12, a single point measurement would appear to be adequate to provide a very good estimate to compute combustor acoustic power via coherence relations with the far-field. The results obtained here for acoustic power are certainly within the scatter of the data used to generate the various empirical prediction schemes.

SUMMARY OF RESULTS

Coherence measurements were made between the fluctuating pressure in the combustor of a YF-102 turbofan engine and far-field acoustic pressure over a range of far-field angles and engine operating conditions. The coherence functions were then used in conjunction with the far-field spectra to compute the combustor-associated far-field noise in terms of sound pressure level spectra, directivity, acoustic power spectra and total acoustic power.

The results indicated a peak in the combustion-associated far-field noise spectrum near 125 Hz at all angles and operating conditions with virtually no far-field combustor-associated noise at frequencies beyond about 250 Hz. The overall sound pressure level directivity patterns peaked near 120^{o} and agreed well with several empirical predictions available in the literature. Individual directivity patterns, however, for certain frequencies (multiples of 40 Hz) while still peaking near 120^{o}, also displayed a 7-8 dB dip near the 60^{o} angle. This apparently anomalous result could not be resolved in view of the low frequencies involved.

The combustor-associated far-field sound pressure spectra were numerically integrated to obtain acoustic power spectra. These were shown to have a peak frequency of 125 Hz, which was relatively insensitive to operating speed. The power spectral shapes, however, did change with operating speed, containing increasing amounts of energy at the higher frequencies. The combustor-associated far-field acoustic power levels were found to be somewhat lower than those predicted by most of the empirical schemes with which they were compared, and also somewhat lower (5-8 dB) than obtained by integration of the directly measured low frequency far-field data.

APPENDIX

The purpose of this appendix is to discuss some of the statistical uncertainties in the data presented in this paper. These statistical errors are an inevitable byproduct of random data analysis techniques and, for the most part, cannot be entirely eliminated from the resulting data.

Computational Scheme

The digital signal processor used to obtain the results presented in this paper digitized each sample record of data into 1024 words at a sampling rate 2.048 times the highest frequency (f_m) selected for analysis:

$$f_{sample} = 2.048\, f_m$$

The processor memory period, or sample record length, therefore, is:

$$T = \frac{\text{No. of words/record}}{\text{No. of words/second}}$$

$$= 1024/(2.048\, f_m) = 500/f_m \quad \text{seconds/record} \qquad \text{(A1)}$$

Since the number of words/record is fixed, the resolution bandwidth is

$$B_e = 1/T = f_m/500$$

The number of statistical degrees of freedom per sample record, therefore is (ref. 10)

$$n = 2B_eT = 2\,(f_m/500)(500/f_m) = 2 \qquad \text{(A2)}$$

So, if N independent sample records are averaged, the total number of statistical degrees of freedom in the average is

$$n_{TOT} = 2N \tag{A3}$$

For a total tape record length of 120 seconds, the maximum number of independent sample records is

$$N = 120/T \tag{A4}$$

Bias Error Due to Time Delay

In the usual analysis of signal pairs, the similarities, or mutual properties between the two signals do not coincide with one another until some time period has elapsed. In the present investigation, of course, this is the acoustic propagation time between the combustor and the far-field, which was shown in references 3 and 6 to be about 87 msec.

As pointed out in reference 13, failure to account for this time delay leads to a bias error in the coherence function, which becomes underestimated. The best procedure to eliminate or minimize this bias error is to delay the signal that occurs earlier in time, thus allowing the later signal to "catch up" before implementing any computation. The processor used to obtain the results shown in this paper, however, did not have such a precomputation delay feature when computing coherence functions. The bias error, therefore, was calculated and the correction applied to the overall power levels. From (13), the bias error due to time delay is given by

$$\gamma^2_{CF}(f)/\gamma^2_{CF}(f) = \left(1 - \frac{\tau}{T}\right)^2 \tag{A5}$$

where

$\hat{\gamma}^2_{CF}(f)$ = estimated (i.e., measured) value of the coherence function between combustor and far-field, at the frequency f

$\gamma^2_{CF}(f)$ = true value of the coherence function

τ = delay time between the two signals

T = processor memory period

It is obvious from (A5) that to minimize this bias error, T should be made as large as possible. From equations (A3) and (A4), however, to increase the number of statistical degrees of freedom, and therefore minimize random error (see below), T should be made as small as possible. Any selection of T, therefore, in computing the coherence function, represents a compromise. For the results shown in this paper, f_m was chosen at 400 Hz. So, from (A1),

$$T = 500/400 \text{ Hz} = 1.25 \text{ seconds/record}$$

Substituting this into (A3)

$$\hat{\gamma}^2_{CF}(f)/\gamma^2_{CF}(f) = \left(1 - \frac{.087}{1.25}\right)^2 = 0.866$$

The measured values of the coherence function, therefore, are about 87 percent of the true values. In terms of decibels, then, this represents an error of about 10 log (1/0.866) = 0.6 dB. This amount was added to the overall combustor far-field power levels shown in figure 12 and in the appropriate column of table I, in the text.

Coherence Function Confidence Limits

Because of the finite sample length of the data, there is a variance (i.e., random) error in the computation of the coherence functions. There are also bias errors due to finite bandwidth.

The confidence limits on the coherence function estimate due to these errors may be calculated, to a close degree of approximation, from: (ref. 14):

$$\tanh [w(f) - (n_{TOT} - 2)^{-1} b(f) - \sigma_w Z_{\alpha/2}] < \gamma_{CF}(f)$$

$$\leq \tanh [w(f) - (n_{TOT} - 2)^{-1} b(f) + \sigma_w Z_{\alpha/2}] \qquad (A6)$$

where

$w(f) = \tanh^{-1} [\hat{\gamma}_{CF}(f)]$

n_{TOT} = number of statistical degrees of freedom in the estimate = 2N

$b(f) = [\gamma_{CF}(f) + 1.1]/2[\gamma_{CF}(f) + 0.1]$

$\sigma_w = \sqrt{1/(n_{TOT} - 2)}$

$Z_{\alpha/2}$ = The $100\alpha/2$ percentage point of the standardized normal probability distribution

Note from the above, that to solve for the confidence limits on the coherence function estimate, $\hat{\gamma}^2_{CF}(f)$, the true value, $\gamma^2_{CF}(f)$, must be known. The procedure used here to calculate the confidence limits was to assume that the estimated value could be substituted for the true value in b(f). This is clearly adequate as long as

$$[w(f) \pm \sigma_w Z_{\alpha/2}](n-2) >> b(f) \qquad (A7)$$

Futhermore, to produce a conservative result, the estimated values of $\hat{\gamma}^2_{CF}$ used in (A6) were those obtained before correcting for the time delay bias.

Example:

For 90 percent confidence limits, then $Z_{\alpha/2} = 1.645$ (see any table of the standardized normal probability distribution). For the present work with a 120 second taped record, and T = 1.25 seconds, then

$$N = 120/T = 120 \text{ seconds}/1.25 \text{ seconds} = 96 \text{ averages}$$

$$n_{TOT} = 2\,(96) = 192$$

$$(n_{TOT}-2)^{-1} = 1/190 = 0.00526$$

$$\sigma_w = \sqrt{1/(n_{TOT} - 2)} = 0.0726$$

For a measured coherence $\hat{\gamma}^2_{CF}(f)$ of, say, 0.5, we have:

$$w(f) = \tanh^{-1}\left(\sqrt{0.5}\right) = 0.881$$

$$b(f) = \left(\sqrt{0.5} + 1.1\right)/2\left(\sqrt{0.5} + 0.1\right) = 1.119$$

Substituting these into (A6), gives:

$$\tanh\,[0.881 - 0.00526\,(1.119) - 0.0726\,(1.645)] < \gamma_{CF}(f)$$

$$\leq \tanh\,[0.881 - 0.00526\,(1.119) + 0.0726\,(1.645)]$$

or,

$$0.407 < \gamma^2_{CF}(f) \leq 0.576$$

or, in decibels, referenced to the estimate

$$-0.89 \text{ dB} < 10 \log \frac{\gamma^2_{CF}(f)}{\hat{\gamma}^2_{CF}(f)} \leq +0.61 \text{ dB}$$

So, for any measured coherence value of 0.5, the associated combustor coherence spectrum has a 90 percent limit of about -0.9 dB to +0.6 dB. just due to the variance in $\hat{\gamma}^2_{CF}(f)$.

For lower values of the measured coherence function, the confidence limits are wider. For example, at a measured coherence of 0.1, calculations identical to the above produce 90 percent confidence limits of -2.7 dB to +1.8 dB. In both case above, it can be verified that the inequality given by (A7) is satisfied.

Combustor Coherence Spectrum Confidence Limits

The directivity and power results shown in this paper were obtained by multiplying the measured coherence function by the far-field spectrum, on a frequency by frequency basis. The statistical errors in the coherence functions were described above. There also are, however, statistical errors associated with the far-field spectral estimate. These errors combine (though not in an additive fashion) with the errors in the coherence estimate to produce the final error in the combustor coherence spectra. In reference 10, it is shown the variance error, ϵ_r, in spectral estimates obtained by FFT techniques such as used here is given by:

$$\epsilon_r [\hat{G}_{FF}(f)] = \sqrt{\frac{2}{n_{TOT}}}$$

where $\hat{G}_{FF}(f)$ is the far-field spectral estimate.

For the present case, N = 64 (the far-field spectra were computed independently, and the number of averages was required to be a power of 2). So, the error is approximately 12.5 percent or about 0.5 dB. This error prevails throughout the spectral range because of the constant bandwidth. This is in contrast to an error band of at least 1.5 dB associated with the coherence function estimate. In reference 13 it is shown that for cases such as this, when one error is significantly larger than the other, the larger error dominates the final coherence spectrum estimate. With the assumption that the variance errors in the combustor

coherence spectra are dominated by the variance errors in the coherence function, figure A1 shows a typical combustor coherence spectrum with the associated 90 percent confidence limits sketched in. This figure is for 43 percent engine speed and a far-field microphone angle of 120^{o}. It is representative of all the results obtained in this paper.

The bias errors in the far-field spectral estimates are proportional to the resolution bandwidth, which for this case has an effective value of 1 Hz. Because the far-field spectra were all smoothly varying (i.e., no tones), these bias errors may be considered negligible.

REFERENCES

1. Hoch, R. G., Thomas, P., and Weiss, E., "An Experimental Investigation of the Core Engine Noise of a Turbofan Engine," AIAA Paper 75-526, Hampton, Va., 1975.

2. Gerend, R. P., Kumasaka, H. A., and Roundhill, J. P., "Core Engine Noise," AIAA Paper 73-1027, Seattle, Wash., 1973.

3. Reshotko, M., et al, "Core Noise Measurements on a YF-102 Turbofan Engine," AIAA Paper 77-21, Los Angeles, Calif., 1977.

4. Mathews, D. C. and Peracchio, A. A., "Progress in Core Engine and Turbine Noise Technology," AIAA Paper 74-948, Los Angeles, Calif., 1974.

5. Burdsall, E. A., Brochu, F. P., and Scaramella, V. M., "Results of Acoustic Testing of the JT8D-109 Refan Engines," Pratt & Whitney Aircraft, East Hartford, Conn., PWA-5298, 1975; also NASA CR-134875.

6. Karchmer, A. and Reshotko, M., "Core Noise Source Diagnostics on a Turbofan Engine Using Correlation and Coherence Techniques," NASA TM X-73535, 1976.

7. Huff, R. G., Clark, B. J., and Dorsch, R. G., "Interim Prediction Method for Low-Frequency Core Engine Noise," NASA TM X-71627, 1974.

8. Mathews, D. C., Rekos, N. F., Jr., and Nagel, R. T., "Combustion Noise Investigation," Pratt & Whitney Aircraft, East Hartford, Conn., PWA-5478, 1977; FAA-RD-77-3.

9. Matta, R. K., Sandusky, G. T., and Doyle, V. L., "GE Core Engine Noise Investigation, Low Emission Engines," Department of Transportation, Washington, D.C., 1977; FAA-RD-77-4.

10. Bendat, J. S. and Piersol, A. G., Random Data: Analysis and Measurement Procedures, John Wiley & Sons, Inc., New York, 1971.

11. Strahle, W. L., Muthukrishnan, M., and Neale, D. N., "Coherence Between Internal and External Noise Generated by Gas Turbine Combustors," AIAA Paper 77-20, Los Angeles, Calif., 1977.

12. Ho, P. Y. and Tedrick, R. N., "Combustion Noise Prediction Techniques for Small Gas Turbine Engines," Inter-Noise 72; International Conference on Noise Control Engineering, Inst. Noise Control Eng., New York, 1972, pp. 507-512.

13. Halvorsen, W. G. and Bendat, J. S., "Noise Source Identification Using Coherent Output Power Spectra," Sound and Vibration, Vol. 9, Aug. 1975, pp. 15, 18-24.

14. Enochson, L. D. and Goodman, N. R., "Gaussian Approximation to the Distribution of Sample Coherence," Air Force Flight Dynamics Lab., Wright Patterson AFB, Ohio, AFFDL-TR-65-57, 1965.

TABLE I - OVERALL POWER LEVEL

(dB, Re: 10^{-13}w)

Engine speed, percent	Ref. (7)	Ref. (8)	Ref. (9)	Direct far-field measurement	Coherence measurements
30	128.7	120.9	127.0	125.0	120.0
43	133.2	122.7	131.5	128.2	123.5
60	137.7	126.3	136.0	134.5	126.2

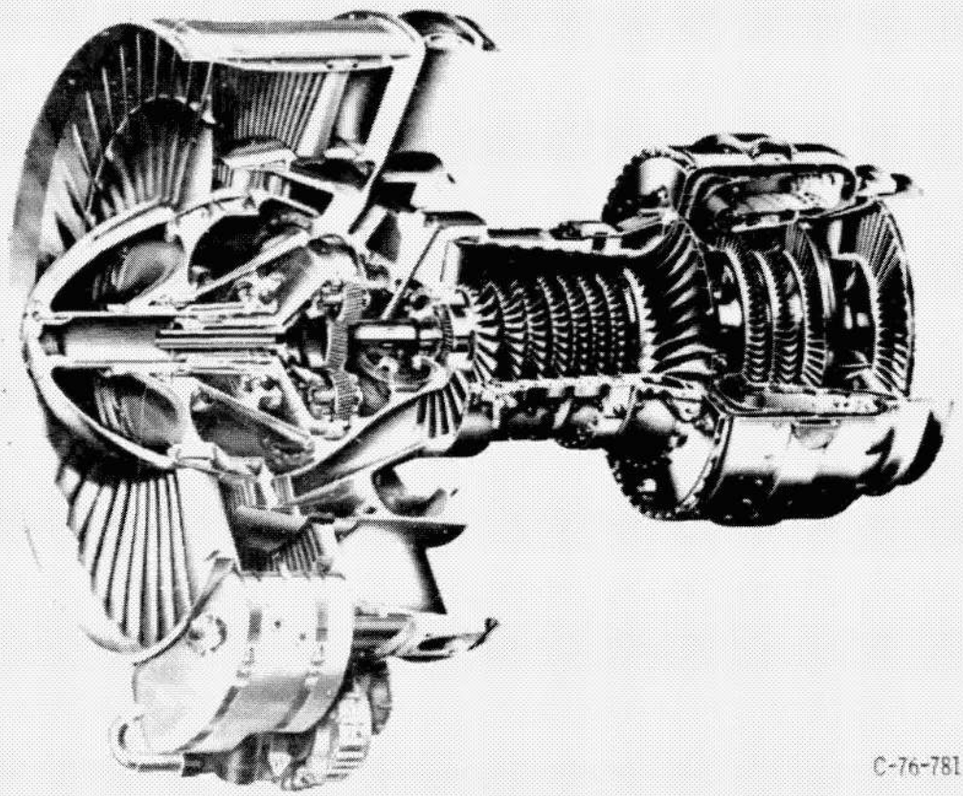

C-76-781

Figure 1. - Cutaway illustration of YF-102 turbofan engine.

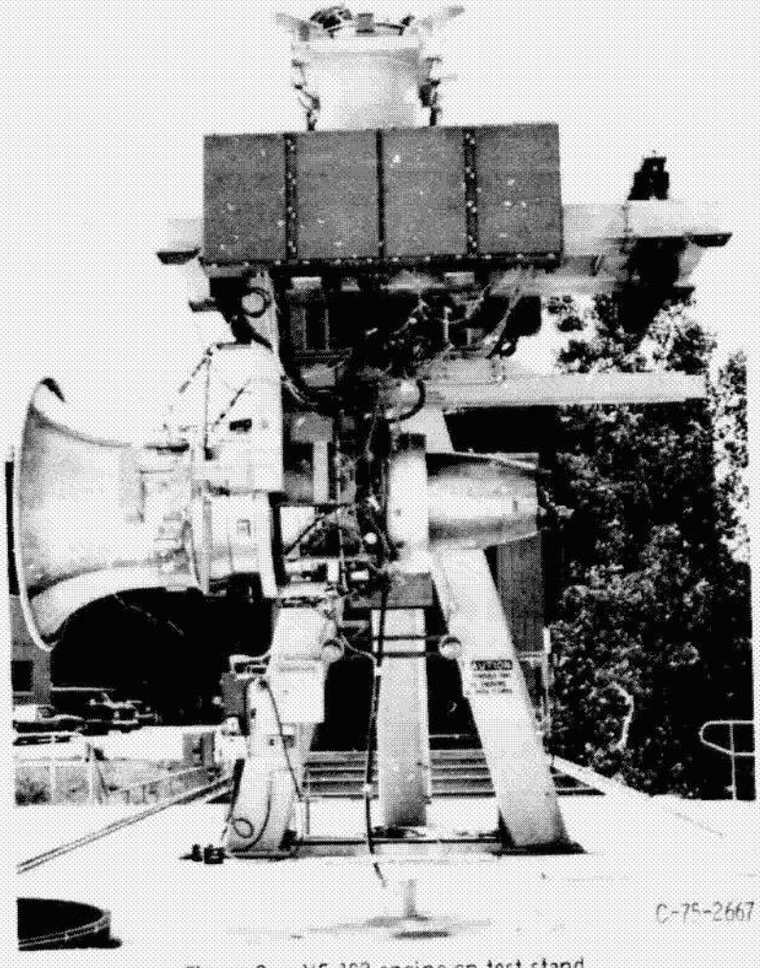

Figure 2. - YF-102 engine on test stand.

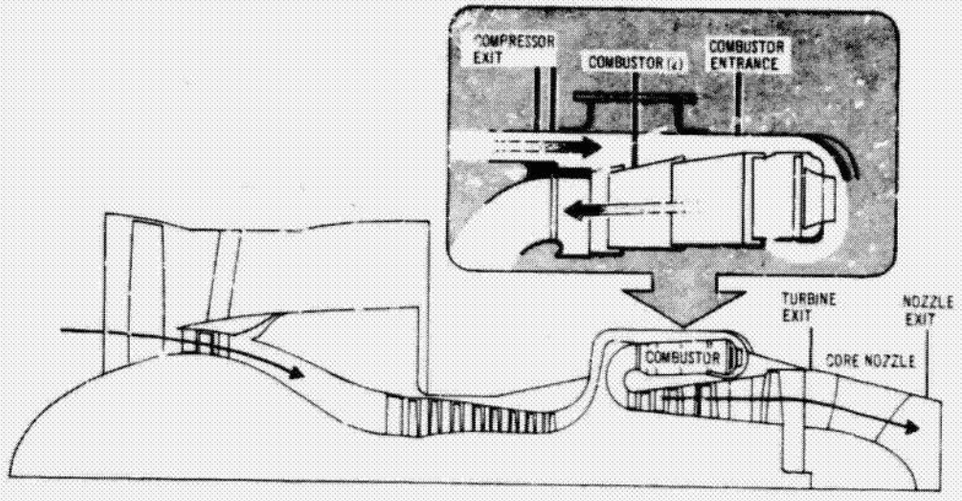

Figure 3. - Core pressure probe locations.

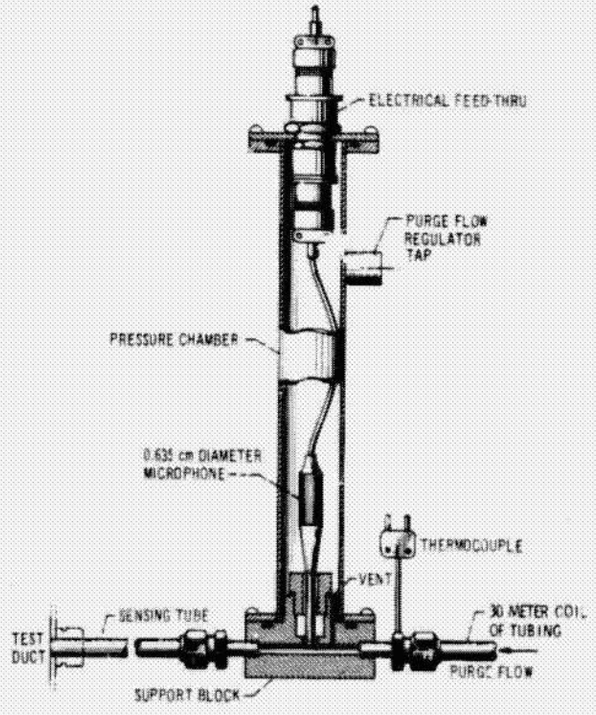

Figure 4. - Core pressure probe.

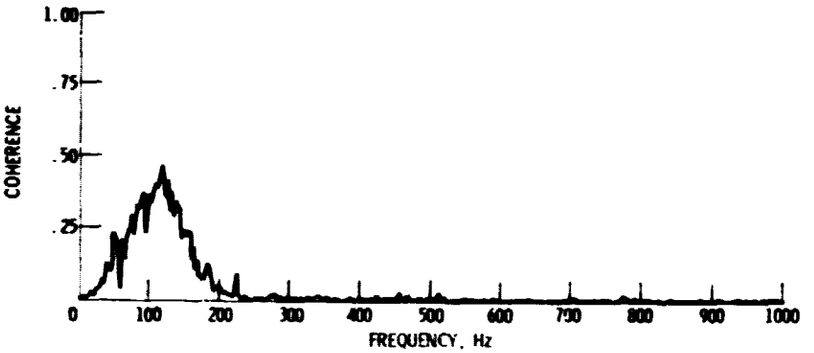

Figure 5. - Coherence between fluctuating combustor pressure and 120° far-field acoustic pressure at 43 percent speed (bandwidth = 2.0 Hz).

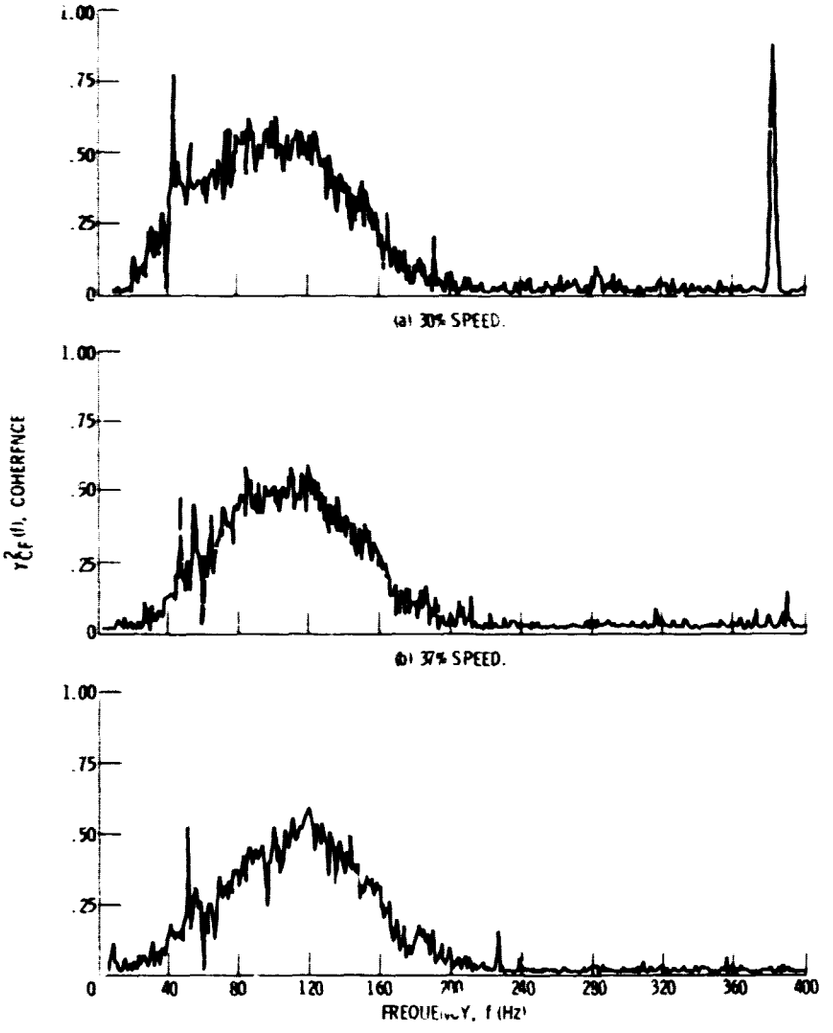

Figure 6. - Coherence between fluctuating combustor pressure and 120° far-field acoustic pressure for several engine speeds (bandwidth = 0.8 Hz).

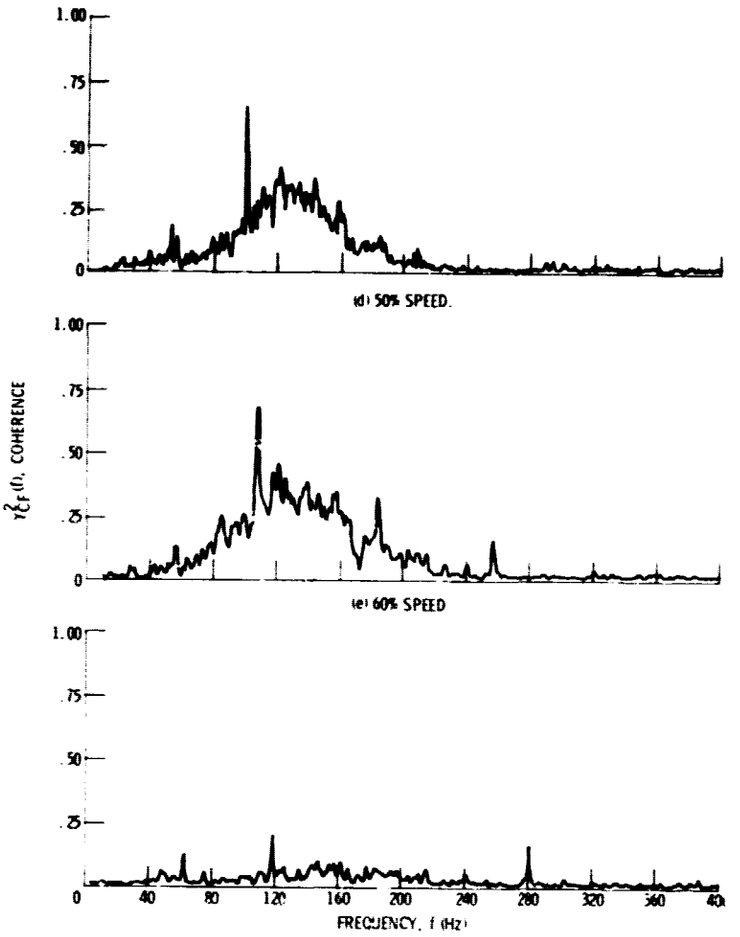

Figure 6. - Concluded.

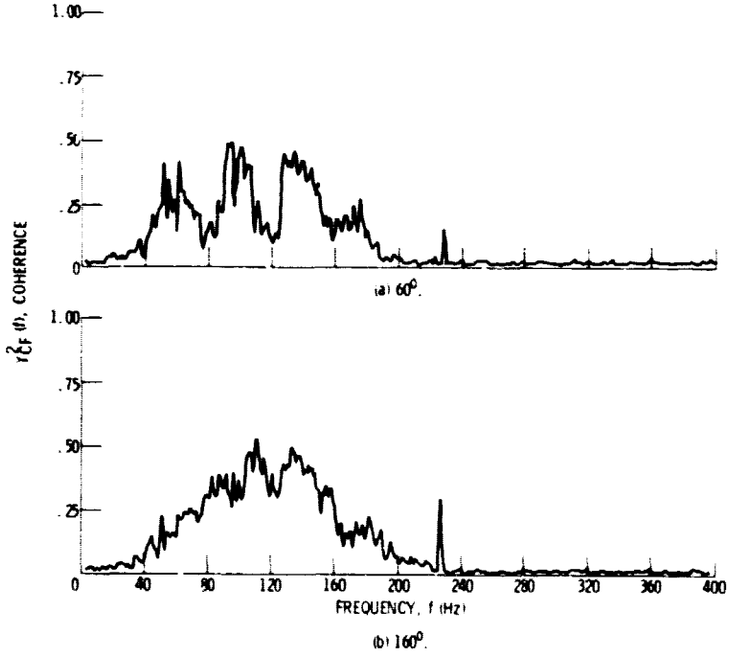

Figure 7. - Coherence between fluctuating combustor pressure and far-field acoustic pressure at 43 percent speed (bandwidth = 0.8 Hz).

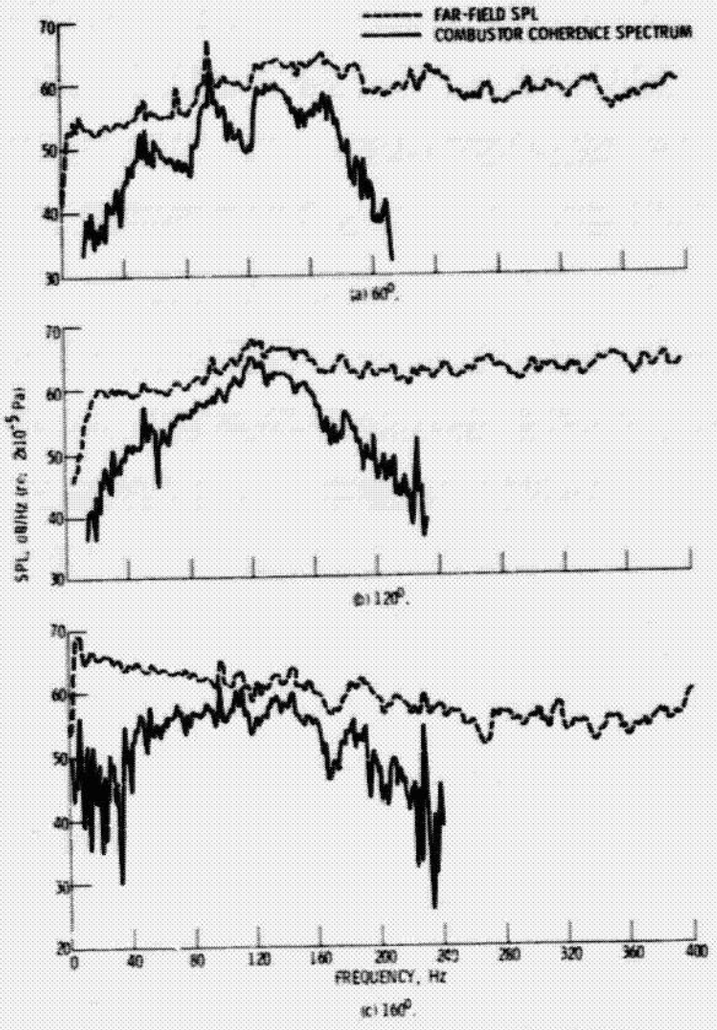

Figure 8. - Far-field SPL and combustion coherence spectra at 43% speed.

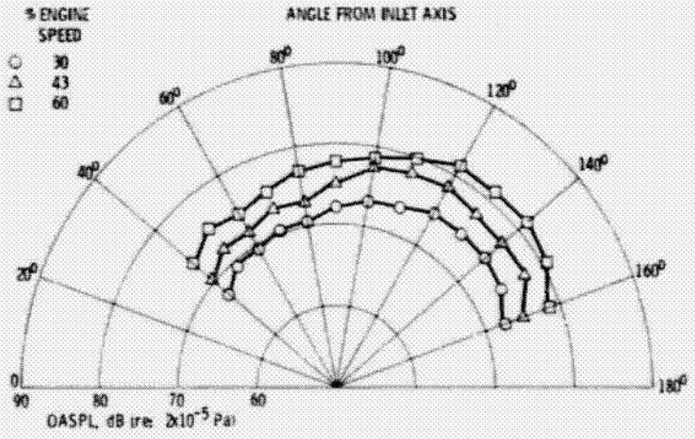

Figure 9. - Combustion noise overall sound pressure level radiation patterns.

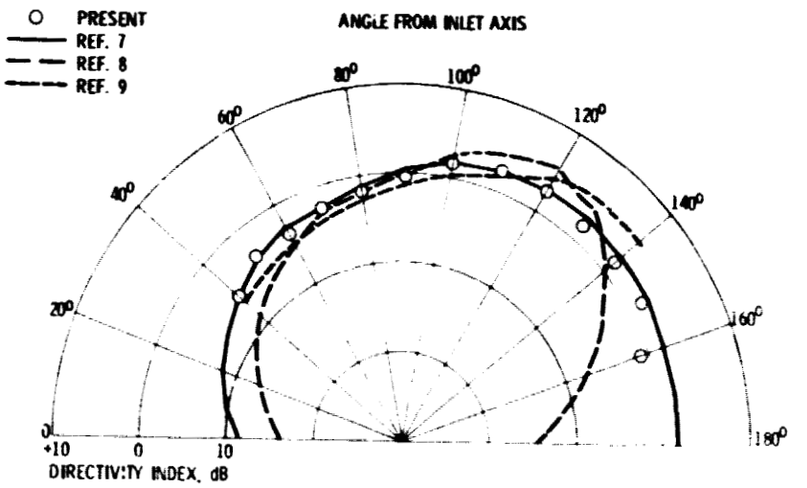

Figure 10. - Combustion noise OASPL directivity index.

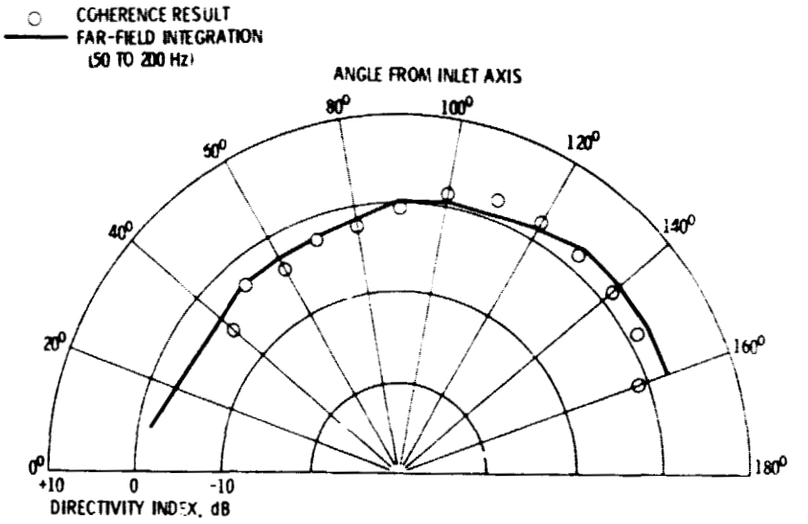

Figure 11. - Comparison of combustion noise OASPL directivity index obtained from coherence spectra and from direct far-field measurement.

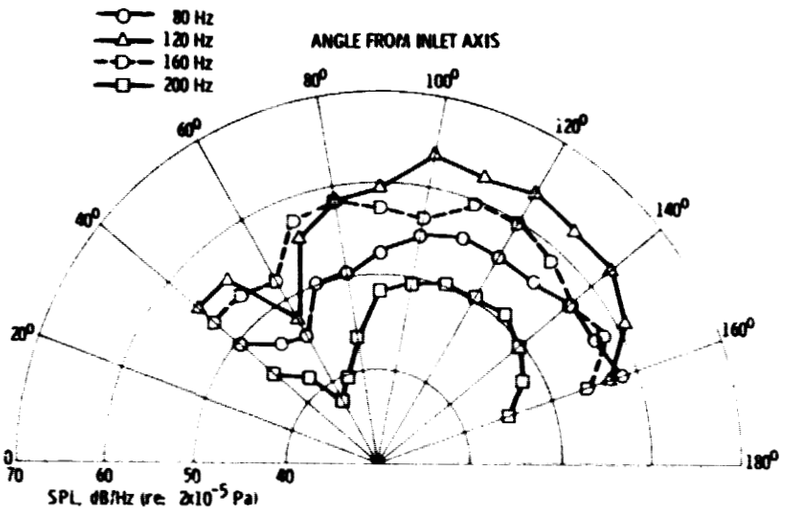

Figure 12. - Directivity pattern of combustion noise SPL for several frequencies.

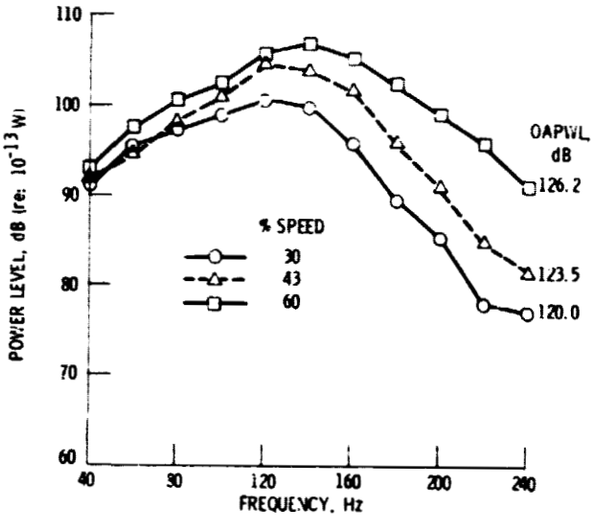

Figure 13. - Combustion noise acoustic power level.

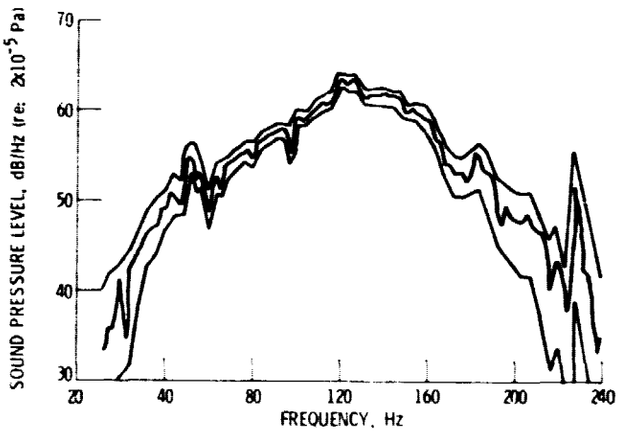

Figure A1. - 90% confidence limits on combustion noise coherence spectrum for 120° position; 43% engine speed; distance = 30.5 m.